Volume 9
Number 33
7 September 2021
Pages 17557–18008

Journal of Materials Chemistry A

Materials for energy and sustainability

rsc.li/materials-a

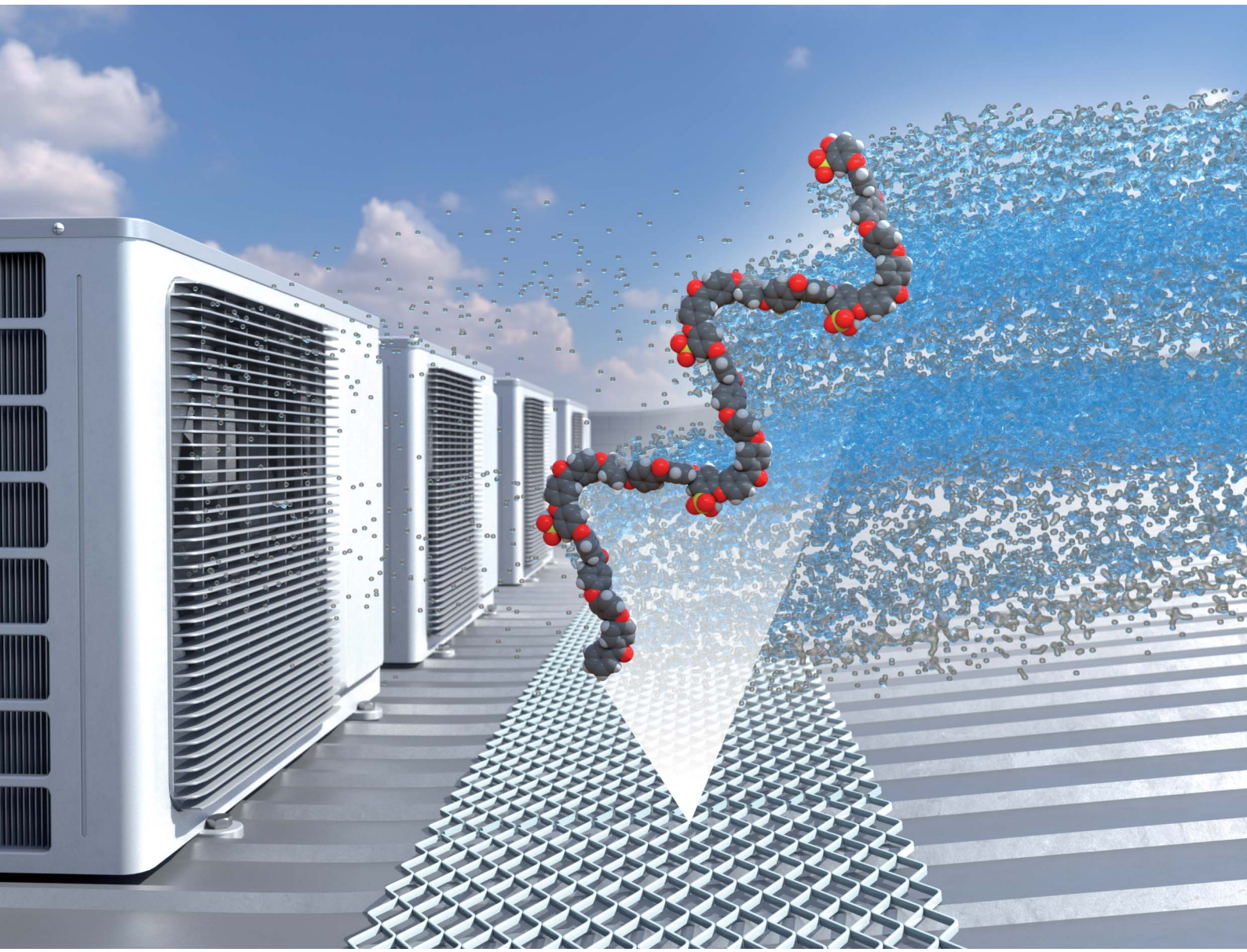

ISSN 2050-7488

ROYAL SOCIETY OF CHEMISTRY

PAPER

Gyorgy Szekely *et al.*

Defining sulfonation limits of poly(ether-ether-ketone) for energy-efficient dehumidification

Journal of Materials Chemistry A

ROYAL SOCIETY OF CHEMISTRY

PAPER

View Article Online
View Journal | View Issue

Open Access Article. Published on 06 Juli 2021. Downloaded on 13.02.26 17:52:21.
This article is licensed under a Creative Commons Attribution 3.0 Unported Licence.

Check for updates

Cite this: J. Mater. Chem. A, 2021, 9, 17740

Defining sulfonation limits of poly(ether-ether-ketone) for energy-efficient dehumidification†

Faheem Hassan Akhtar, ‡[a] Mahmoud A. Abdulhamid, ‡[b] Hakkim Vovusha, [c] Kim Choon Ng, [a] Udo Schwingenschlögl [c] and Gyorgy Szekely *[b]

Received 2nd May 2021
Accepted 6th July 2021

DOI: 10.1039/d1ta03690d

rsc.li/materials-a

Dehumidification is a vital process in the cooling industry and has emerged as a promising tool for alleviating the effects of energy-intensive activities. Advanced engineering materials, which can be employed in dehumidification processes, have attracted considerable attention. However, the majority of commercial adsorbents suffer from low sorption performance in arid climates. In this work, sulfonated poly(ether-ether-ketones) (SPEEKs) were designed as desiccants for dehumidification processes. The *in silico* and experimental investigations at a molecular level enabled the development of desiccants exhibiting outstanding water uptake capacity of more than 300%, fast sorption uptake, and high transport rate. The sorption capacity of the prepared materials outperformed those of the previously reported desiccants. Membrane performance analyses demonstrated remarkably high water vapor permeability and selectivity; therefore, the desiccants developed herein showed potential for application in water vapor control and dehumidification processes in enclosed or confined spaces. Contrary to common assumptions, the correlation between the sulfonation degree and dehumidification performance showed a plateau after maximum curvature. The results of this study open new directions for tailoring energy-efficient materials for dehumidification processes.

Introduction

Removal of moisture from various humidity sources is an essential yet energy-intensive process in both domestic and industrial settings. Different dehumidification methods have been used to control humidity in food storage and air conditioning (AC) systems.[1–3] According to the recent reports by the International Energy Agency and American Society of Heating, Refrigerating and Air-Conditioning Engineers, space cooling accounts for 37–38% of the total residential energy consumption in the US.[4] This vast consumption is attributed to conventional AC systems, which are based on vapor compression cycles. Such devices dehumidify the air by cooling it below the dew point. The process involves condensation, followed by reheating of the air stream, leading to high energy consumption.[5] Consequently, novel energy-saving technologies for dehumidification are highly sought-after.[6–9]

To achieve an acceptable balance between adequate humidity levels and energy consumption, the development of systems exhibiting efficient humidity control is essential. An ideal dehumidification material should have the ability to effectively remove moisture, *i.e.*, it should demonstrate high water uptake and fast sorption kinetics and be capable of driving sorption–desorption transitions. The search for such materials is aimed at alleviating the challenges associated with conventional cooling technologies and engineering cost-effective and energy-efficient dehumidification systems. In this respect, the most widely used adsorbents include zeolites,[10] silica,[11] and metal–organic frameworks (MOFs).[12–15] However, most of these materials suffer from low water uptake and their regeneration methods are impractical. Although MOFs exhibit tunable properties, compared with commercial polymers, they are relatively expensive, limiting their large-scale applications.[12,16]

Recently, owing to their high physicochemical stability, easy scalability, and tunable functionality, polymers have attracted considerable attention. These include porous and perfluoro polymers as well as polymers of intrinsic microporosity.[17–21] However, perfluorinated materials are costly, hindering their large-scale applications. Owing to its high thermal and chemical stability, poly(ether-ether-ketone) (PEEK) is a high-performance polymer. Notably, sulfonated PEEK derivatives (SPEEKs) are inexpensive alternatives to perfluoro polymers.[22] The incorporation of sulfonate moieties into PEEKs enables

[a]Water Desalination and Reuse Centre, King Abdullah University of Science and Technology (KAUST), Thuwal 23955-6900, Saudi Arabia

[b]Advanced Membranes and Porous Materials Centre, King Abdullah University of Science and Technology (KAUST), Thuwal 23955-6900, Saudi Arabia. E-mail: gyorgy.szekely@kaust.edu.sa; Web: www.szekelygroup.com

[c]Physical Science and Engineering Division (PSE), King Abdullah University of Science and Technology (KAUST), Thuwal 23955-6900, Saudi Arabia

† Electronic supplementary information (ESI) available: Polymer characterization, simulation, and kinetic study. See DOI: 10.1039/d1ta03690d

‡ Both authors contributed equally to this work.

This journal is © The Royal Society of Chemistry 2021

Open Access Article. Published on 06 Juli 2021. Downloaded on 13.02.26 17:52:21.
This article is licensed under a Creative Commons Attribution 3.0 Unported Licence.

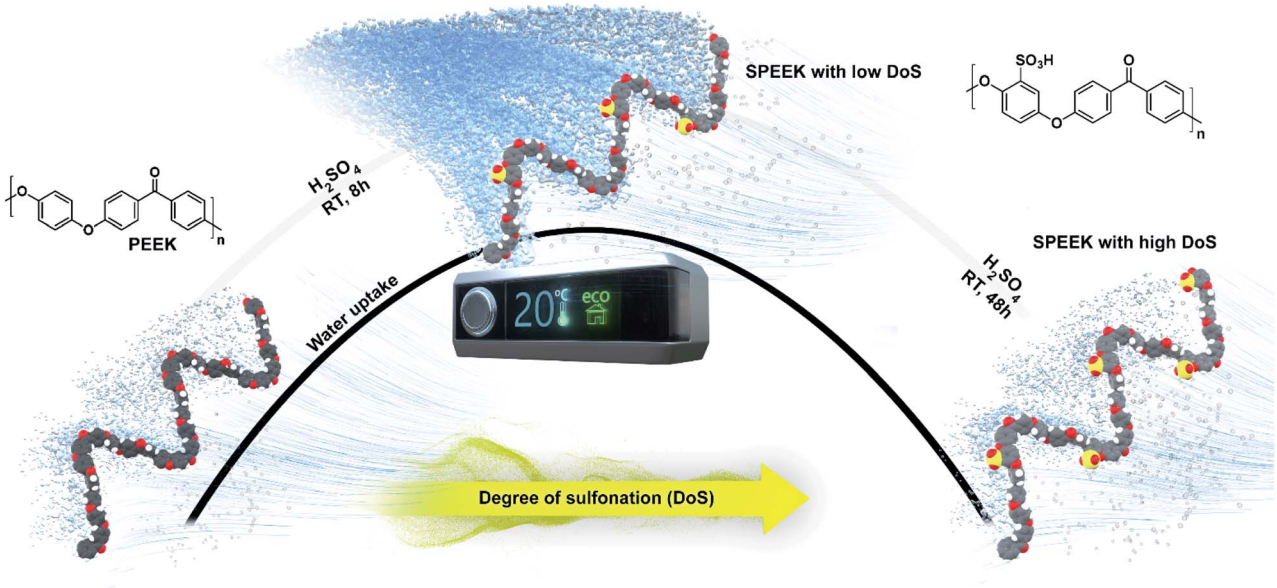

Fig. 1 Schematic illustration of the hypothesis: the degree of sulfonation of SPEEKs does not monotonously increase the water uptake. The concept is validated through PEEK sulfonation at different reaction times, resulting in different degrees of sulfonation.

their utilization in dehumidification processes.[23] In this work, we hypothesized that the degree of sulfonation (DoS) was not linearly correlated with the dehumidification performance (Fig. 1). Thus, despite the common assumption, we aimed to demonstrate that higher DoS limits do not necessarily lead to enhanced activity.

Experimental details

Polymer synthesis

SPEEKs with different DoS were prepared by reacting 280 mg of PEEK (4000P VESTAKEEP obtained from Victrex, UK) with 2 mL of sulfuric acid (95.0–98.0% purchased from Sigma-Aldrich, USA) at room temperature. The reaction was stirred at 150 rpm for a designated time (variable time intervals between 1 and 48 h). The reaction mixture was subsequently poured into deionized water at 0 °C and stirred for 24 h. The water was changed multiple times to obtain a neutralized medium with a pH of 7. The polymer was filtered and dried under vacuum for 24 h at room temperature. Seven polymers with varying DoS were synthesized and denoted as P1–P7. Benchmark non-sulfonated PEEK was denoted as P0 (Table S1, ESI†).

Polymer characterization

The Fourier transform-infrared (FTIR) spectra of the polymers were acquired using a Thermo Nicolet iS10 FTIR spectrometer (Thermo Fisher Scientific, USA) equipped with a diamond head. To enable accurate comparison of the data, the FTIR measurements were performed using the same polymer quantity and the exact number of scans. Thermal gravimetric analysis (TGA) was conducted using TGA 5500 (TA Instruments Inc., USA) to study the decomposition temperature of the prepared SPEEKs. Before the analysis, the samples were dried at 100 °C, followed by heating at a ramp rate of 5 °C min^{-1} up to 600 °C. The glass transition temperature was evaluated using differential scanning calorimetry (DSC) (Model Q2000, TA Instruments Inc., USA) at a ramp rate of 5 °C min^{-1} up to 350 °C. Wide-angle X-ray diffraction (WAXD) analysis was conducted on a Bruker D8 Advance diffractometer (Bruker, USA) from 8° to 40° at a scanning rate of 0.5° min^{-1}. The d-spacing between the polymer chains was calculated according to the Bragg's law ($n\lambda = 2d \sin \theta$). A Mettler Toledo density measurement kit was used to determine the polymer densities based on the Archimedes principle using petroleum ether ($\rho = 0.64$ g mL^{-1}) as the reference liquid at room temperature. A Thermo Scientific™ FLASH 2000 CHNS/O analyzer (Thermo Fisher Scientific, USA) was employed to measure the atomic percentage composition of the polymer samples. The atomic percentage composition was then used to obtain the DoS.

One dimensional (1D) ^{1}H MAS, solid state NMR spectra were recorded on a Bruker AVANCE III spectrometer operating at 600 MHz resonance frequency for ^{1}H utilizing a 3.2 mm double resonance probe. Dry nitrogen gas was utilized for sample spinning to prevent degradation of the samples. NMR chemical shifts are reported with respect to the external references TMS and adamantane. The delay between the scans was set to 4 s to allow the complete relaxation of the ^{1}H nuclei and the number of scans was 8 for ^{1}H.

Two-dimensional double-quantum (DQ) experiments were recorded on a Bruker AVANCE III spectrometer operating at 600 MHz with a conventional double resonance 3.2 mm CP/MAS probe, according to the following general scheme: excitation of DQ coherences, t_1 evolution, z-filter, and detection. The spectra were recorded in a rotor synchronized fashion in t_1 by setting the t_1 increment equal to one rotor period (45.45 μs). One cycle of the standard back-to-back (BABA) recoupling

Open Access Article. Published on 06 Juli 2021. Downloaded on 13.02.26 17:52:21.
This article is licensed under a Creative Commons Attribution 3.0 Unported Licence.

sequences was used for the excitation and reconversion period. Quadrature detection in w_1 was achieved using the States-TPPI method. An MAS frequency of 22 kHz was used. The 90° proton pulse length was 2.5 μs, while a recycle delay of 5 s was used. A total of $128t_1$ increments with 128 scans per each increment were recorded. The DQ frequency in the w_1 dimension corresponds to the sum of two single quantum (SQ) frequencies of the two coupled protons and correlates in the w_2 dimension with the two corresponding proton resonances.

Water vapor sorption experiments were conducted on Q5000 SA (TA instruments, USA) using the gravimetric sorption balance method at 25 °C and in a controlled humidity range of 0–95% relative humidity (RH). Before proceeding to the next step, the mass uptake of the polymer samples was equilibrated at a certain humidity. The polymer samples were dried at room temperature for 24 h under vacuum, 90 °C for 5 h in a vacuum oven, followed by *in situ* drying at 70 °C for 5 h before the water vapor sorption analysis. The water vapor sorption kinetics was analyzed at various RHs. The water vapor uptake rate was calculated using a classical approach. Specifically, the time average of water vapor uptake was considered for a specific time interval, which depended on the cycle time of the application. Thus, at the required humidity, the water vapor uptake was summed over the time intervals of 5 and 10 min, *i.e.*, conventional adsorption cycle time, and divided by the same.

Computational details

Density functional theory (DFT) calculations were performed to determine the polymer–polymer and polymer–water interactions on the M062X/6-31+G** level of theory by employing the Gaussian 09 code. The sulfonated polymers with various percentages of water molecules were subjected to molecular dynamics (MD) simulations using the Forcite module of Materials Studio 2019 with the COMPASS force field. Five chains of the sulfonated polymers (each chain consisted of 10 repeat units) were generated and solvated with different numbers of water molecules. A canonical ensemble was used for the 2000 ps simulations at a time step of 1 fs and 300 K. A Nose–Hover thermostat was used to control the temperature during the MD simulations.

Results and discussion

To evaluate the effect of sulfonation on the PEEK performance, seven SPEEKs with different DoS were prepared *via* a direct sulfonation reaction using concentrated sulfuric acid. The reaction time was varied between 1 and 48 h to obtain SPEEKs with varying DoS (Table S2, ESI†). The DoS increased with an increase in the sulfonation reaction time,[24] which reached a maximum of 46%.

The FTIR spectra of all the polymers showed a typical broad absorption band at 3300–3700 cm^{-1}, corresponding to the hydroxyl (–OH) groups and the spectra were similar to the previously reported SPEEK polymers (Fig. 2a).[25–27] Moreover, the symmetric absorption bands of the carbonyl (C=O) groups were detected at 1650 cm^{-1} and was in agreement with the literature.[25]

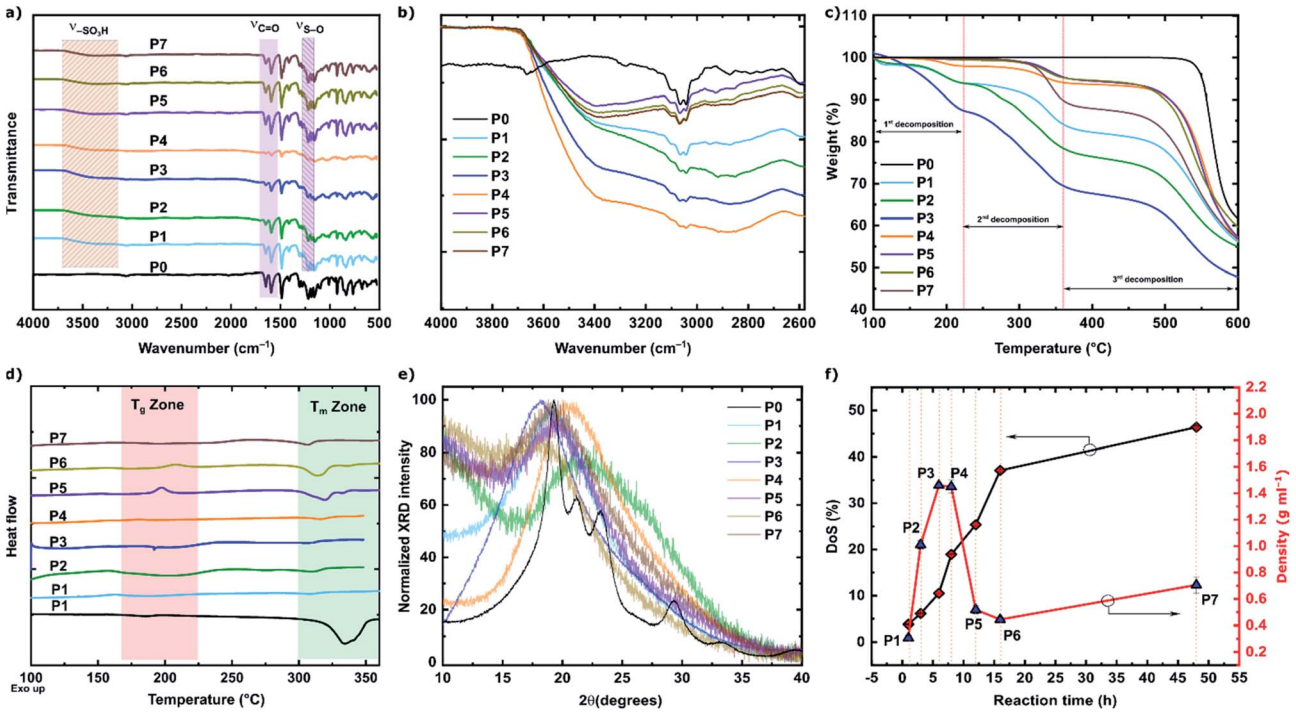

Fig. 2 SPEEK characterization: FTIR spectra in the range of (a) 500–4000 cm^{-1} and (b) 2600–4000 cm^{-1}; (c) thermal degradation obtained using TGA; (d) DSC thermograms at 100–350 °C; (e) WAXD spectra with $2\theta = 8$–40°; and (f) DoS and densities of polymers as a function of the sulfonation reaction time.

Open Access Article. Published on 06 Juli 2021. Downloaded on 13.02.26 17:52:21.
This article is licensed under a Creative Commons Attribution 3.0 Unported Licence.

The appearance of a characteristic absorption band of S–O was observed at 1185 and 1150 cm^{-1}, confirming a successful sulfonation of PEEK.

Intriguingly, the spectrum of SPEEK with a DoS of 18.9% (P4) exhibited the most intense –OH absorption peak in the normalized FTIR spectrum (Fig. 2b). The order of peak intensity was as follows: P4 > P3 > P2 > P1 > P7 > P6 > P5. As previously reported, the strength of the –OH absorption band is related to the number of free –OH groups, which are available to form hydrogen bonding interactions with electron acceptor moieties.[28,29] Additionally, the order of the –OH peak absorption intensity indicated the water sorption capacity of the polymers.

The thermal degradation profiles of SPEEKs obtained using TGA were plotted against those of nonsulfonated PEEK (Fig. 2c). The SPEEK polymers exhibited lower decomposition temperatures than the PEEK polymers owing to the presence of $-SO_3H$ groups in the polymer backbone of the former, which degraded at a lower temperature. The TGA curves of SPEEKs with a DoS of less than 20% (P1–P4) showed three decomposition steps. The first decomposition step (150–220 °C) was attributed to the presence of free $-SO_3H$ moieties exhibiting negligible intramolecular interactions, thus showing a tendency to decompose earlier. However, the second decomposition step (220–360 °C) corresponded to the degradation of $-SO_3H$ moieties, which participated in strong hydrogen bonding interactions. The third degradation step (360–600 °C) was ascribed to the degradation of the polymer backbone (Table S3, ESI†). In contrast, the TGA curves of SPEEKs with a DoS of more than 20% (P5–P7) exhibited only two decomposition steps, indicating the presence of only one type of $-SO_3H$ moiety, which formed strong hydrogen bonding interactions.

The melting point (T_m) of nonsulfonated PEEKs determined from DSC thermograms was 335 °C, higher than that of SPEEKs. The T_m of SPEEKs was 306–319 °C. The decrease in T_m resulted from the introduction of polar $-SO_3H$ groups, which decreased the thermal stability of the polymer. Furthermore, a higher T_m signified a greater strength and rigidity of the polymer chains. The glass transition temperature (T_g) of SPEEKs was 156–186 °C (Fig. 2d, Table S4, ESI†), which was comparable to that of nonsulfonated PEEKs (T_g = 172 °C).

Moreover, the broad 2θ WAXD patterns confirmed the amorphous nature of the synthesized polymers (Fig. 2e). After the incorporation of the $-SO_3H$ moiety into the semicrystalline PEEK backbone, SPEEKs showed amorphous morphology with d spacing ranging from 4.1 to 4.6 Å. Similar findings were previously observed for other types of sulfonated polymers.[30] The difference in the d-spacing between the SPEEKs was marginal attributed to the strong chain packing as well as the presence of planarity in the polymer backbones, which favored chain packing. This finding was in contrast to our previously reported iPEEKs, which demonstrated high internal free volume.[31]

The density of SPEEKs varied depending on the DoS (Fig. 2f). Remarkably, the density increased from 0.306 to 1.46 g mL^{-1} when the reaction time was increased from 1 to 8 h, corresponding to an increase in the DoS from 3.8% to 18.9%.

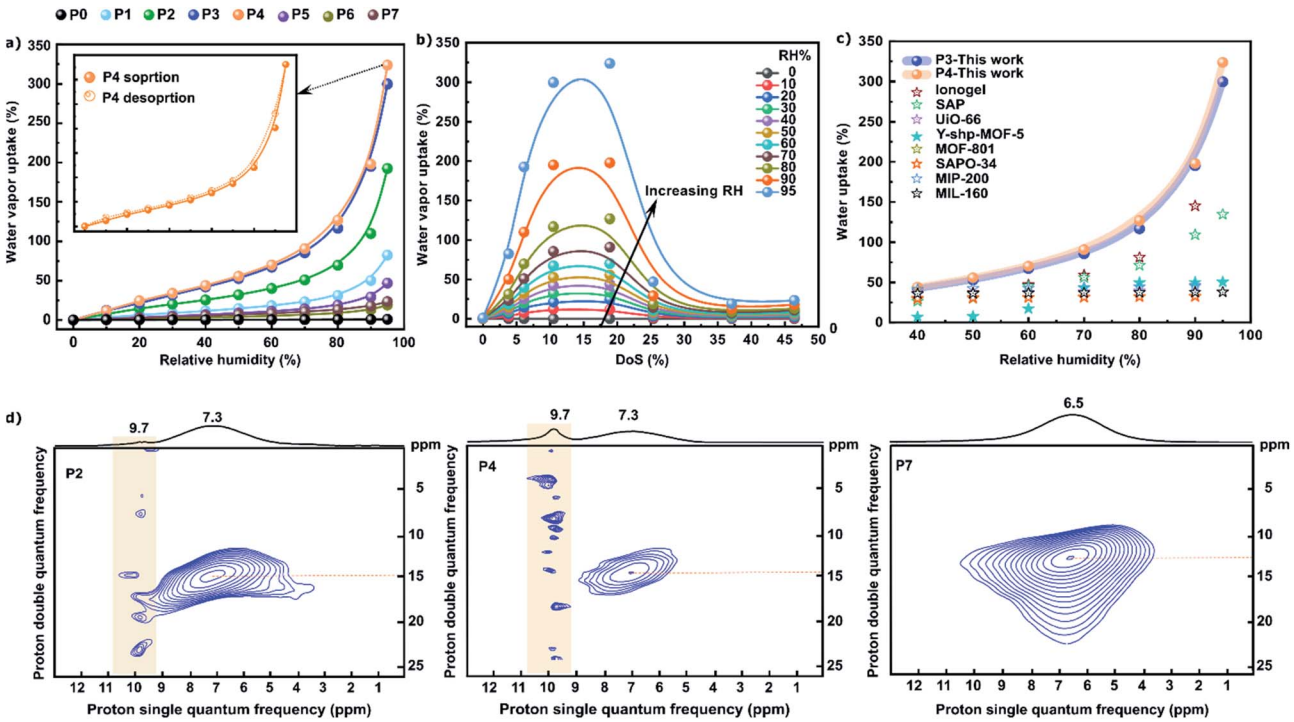

Fig. 3 The search for the highest dehumidification performance: (a) water vapor uptake *vs.* RH for PEEK and SPEEK polymers measured at 25 °C; hysteresis for P4 is shown in the inset; (b) the effect of DoS on the water vapor uptake; (c) comparison of the performance of P3 and P4 relative to the previously reported materials for water uptake, which are summarized in Table S5, ESI;† and (d) solid state ^{1}H NMR spectra of P2, P4, and P7 polymers with low, medium, and high DoS, respectively.

Open Access Article. Published on 06 Juli 2021. Downloaded on 13.02.26 17:52:21.
This article is licensed under a Creative Commons Attribution 3.0 Unported Licence.

However, the density decreased when the reaction time was further increased to 48 h (DoS of 46%) (Table S1, ESI†). The polymer characterization supported our hypothesis regarding the existence of two types of $-SO_3H$ moieties, *i.e.*, one that was free and available to interact with water molecules, and another that was unavailable owing to strong internal hydrogen bonding. Hence, to correlate our findings on the chemical nature of SPEEKs with their dehumidification performance, we conducted water vapor adsorption experiments as well as DFT and MD calculations.

Water vapor sorption isotherms were obtained to experimentally investigate the effect of variations in DoS on the dehumidification performance of SPEEKs (Fig. 3a). The partial pressure of the water vapor was automatically controlled using N_2 as the carrier gas, which was mixed with a wet stream. The nonsulfonated PEEK (P0) showed a low water uptake of less than 1% even at high RH. The sorption increased with RH, and at higher RH, the relaxation phenomenon was attributed to the Fickian diffusion, suggesting the occurrence of dual-mode sorption. SPEEKs exhibited higher water vapor sorption than PEEKs, indicating the presence of hydrophilic sites in the form of $-SO_3H$ moieties on the backbones of the former. P4 with a DoS of 19% exhibited the best performance, and consequently its desorption was also examined. Fig. 3a shows the sorption/desorption isotherms for P4. The minimal hysteresis confirmed the non-swelling behavior of P4, which is a prerequisite for industrial applications. Moreover, during the desorption cycle, water uptake approaches near 0 (1.023%) when the RH is 0, which demonstrates that most of the water can be removed even at low temperature and low RH. The sulfonation of PEEKs significantly affected the water vapor sorption, which varied depending on the DoS (Fig. 3b). Moreover, the water vapor uptake increased as the RH increased because more water molecules could associate with the $-SO_3H$ moieties of SPEEKs. We speculated that the hydration of SPEEKs and increasing humidity resulted in the formation of interconnected channels, which led to fast water vapor sorption. The availability of abundant hydration sites (*i.e.*, $-SO_3H$, C=O, and C–O) also resulted in good hygroscopicity, ultimately increasing the water vapor uptake. The sorption increased as the DoS increased. In the case of P4, the sorption reached a maximum of 320% at a DoS of 19%. At 95% RH, both P3 and P4 showed a water uptake of more than 300% compared with their dry weight, which demonstrated the great potential of the polymers for applications in continuous desiccant-based dehumidification processes. However, a further increase in the DoS from 19% to 46% led to a substantial reduction in the performance, which corresponded to a decrease in sorption from 320% to 24%. Hence, it was deciphered that to achieve the best dehumidification performance, controlling the DoS, rather than maximizing it, is essential. We analyzed the plateau for the water vapor uptake as a function of DoS.

To further examine the performance of the polymers, the obtained water vapor sorption was quantitatively compared with those of the previously reported materials (Fig. 3c). Remarkably, the dehumidification performance of the best-performing SPEEK (P4) was superior to those of the well-known porous polymers and MOFs. Additionally, SPEEKs could operate under humid conditions as an adsorbent-coated

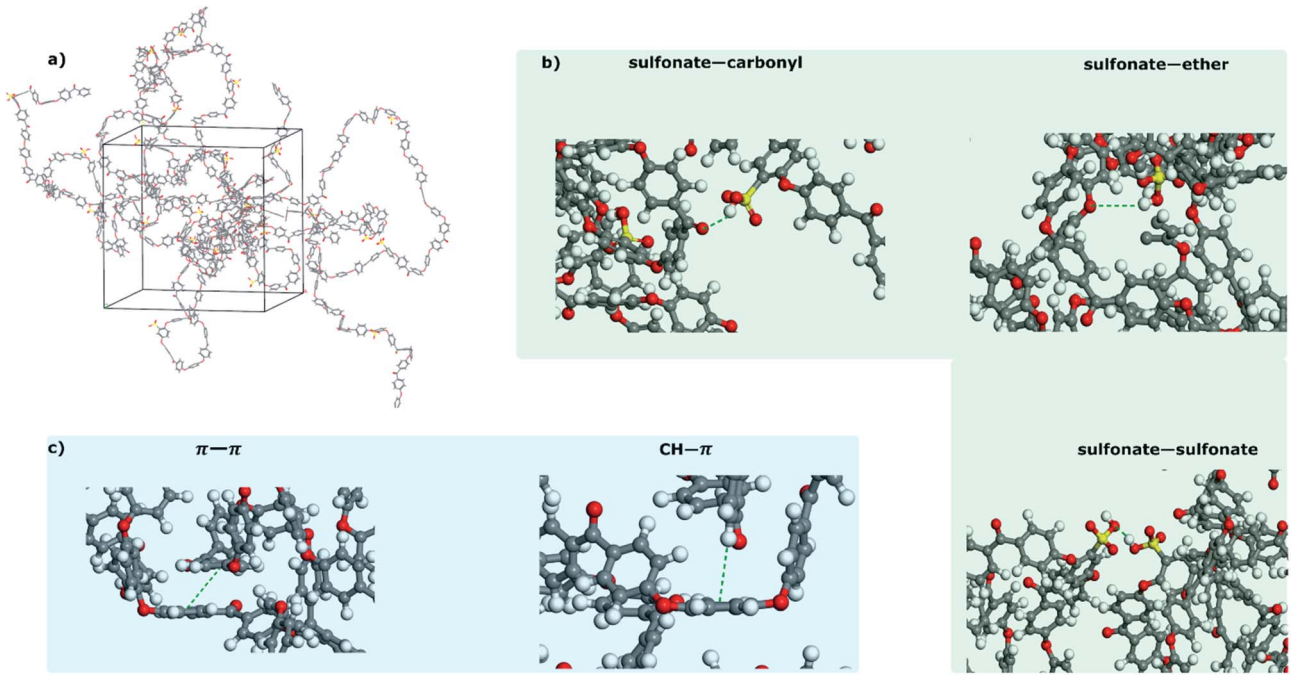

Fig. 4 Molecular level understanding of the SPEEK-based dehumidification system using MD simulations: (a) visual representation of an amorphous cell filled with polymer chains; (b) dominant hydrogen bonding interactions of the $-SO_3H$ moieties in SPEEK chains; (c) minor π interactions.

Open Access Article. Published on 06 Juli 2021. Downloaded on 13.02.26 17:52:21.
This article is licensed under a Creative Commons Attribution 3.0 Unported Licence.

desiccant wheel, surpassing the performance of current state-of-the-art desiccant materials.

Solid state ^{1}H nuclear magnetic resonance (NMR) spectroscopy was previously used to investigate self-association within the sulfonated polymers.[32] Hence, herein, we employed this technique to elucidate the effect of DoS on the availability of free $-SO_3H$ moieties, which can act as adsorption sites for water uptake (Fig. 3d).

Three polymers with low (P2), medium (P4), and high (P7) DoS were selected. The ^{1}H NMR spectrum of P2 with a DoS of 6% revealed several peaks with a medium intensity at 9.7 ppm, corresponding to the active $-SO_3H$ moieties.

As the DoS increased from 6% to 19%, the number of peaks at 9.7 ppm increased, suggesting that the number of active adsorption sites was higher in P4 than in P2. In contrast, the spectrum of P7 with a DoS of 46% showed no distinct peaks at 9.7 ppm. However, a broad peak was observed at 3–11 ppm. The introduction of more $-SO_3H$ moieties into the PEEK backbone led to stronger self-association *via* hydrogen bonding. This resulted in a reduced number of active hydrophilic sites, ultimately decreasing the water uptake. To understand the self-association and water uptake as a function of DoS on a molecular level, we subsequently conducted DFT and MD simulations. To analyze the molecular level interactions between water molecules and polymers, we relaxed the geometry of a single water molecule adsorbed at various binding sites of the polymers.

The minimum energy geometries for the binding of water with the SPEEKs and PEEKs are depicted in Fig. S1 (ESI).† The calculated binding energy of a single water molecule on the SPEEK and PEEK units was −54.16 and −15.25 kJ mol^{-1}, respectively. The obtained binding energy values revealed that SPEEKs exhibited a higher binding affinity toward water molecules than PEEKs owing to a higher number of hydrogen bonds. This was attributed to the presence of $-SO_3H$ moieties in the former and agreed with the experimental dehumidification results.

The MD simulations showed that irrespective of the DoS, the SPEEKs formed both inter and intramolecular hydrogen bonds, including sulfonate–carbonyl, sulfonate–ether, and sulfonate–sulfonate bonds (Fig. 4a–c). Additionally, π–π stacking and CH–π interactions were detected. Notably, hydrogen bonds and π interactions stabilized the polymer system. The hydrogen bonds in the polymer chains became more prominent as the DoS increased (Table S6, ESI†), which supported the hypothesis regarding the decrease in the number of free $-SO_3H$ moieties available for water vapor sorption. Moreover, the variation in the calculated S–S distance (Fig. 5a) followed the same trend as the experimental water vapor uptake (Fig. 3b), confirming that the $-SO_3H$ moieties were the farthest from each other at a DoS of 19%. Consequently, they exhibited fewer interactions within the polymer system, resulting in more $-SO_3H$ moieties available for water vapor sorption. A longer S–S distance favored water sorption because it minimized the hydrogen bonds in the polymer system. In particular, P1 showed an S–S distance of 6.53 Å, which increased as the DoS increased, reaching 20.03 and 20.80 Å for P3 and P4, respectively. However, a further

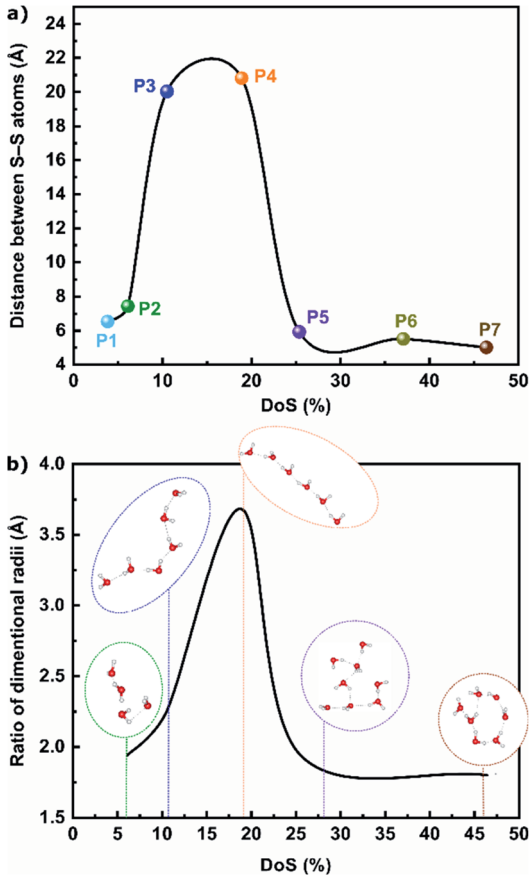

Fig. 5 (a) S–S distance as a function of DoS; and (b) water cluster radii as a function of DoS at 90% RH.

increase in DoS decreased the S–S distance (Fig. S2, ESI†). During water vapor sorption, the self-association of water molecules leads to the formation of polymer clusters and swelling.[33]

During water vapor sorption, the self-association of water molecules leads to the formation of polymer clusters and swelling.[30] Herein, the aggregates of water molecules were observed at less than 70% RH. Typically, water molecules form cyclic structures of varying sizes at less than 90% RH. The formation of water clusters significantly changed as a function of DoS at 90% RH. For instance, P2 with a DoS of 6% showed negligible cyclic cluster formation at 90% RH. The shape of the water clusters changed from cyclic to linear when the DoS increased from 6% to 19%. However, at a DoS of more than 19%, the water cluster became cyclic again and exhibited larger sizes (Fig. 5b). A lower S–S distance in the case of P2, P5, and P7 resulted in the formation of strong hydrogen bonding between the $-SO_3H$ groups and decreased affinity toward water molecules, generating cyclic clusters. The shape of water clusters is expected to have a direct effect on the diffusion coefficients.[34] The linear chain of water molecules in the case of P3 and P4 indicated an increase in the diffusion coefficient (Fig. 6a). However, an increase in the diffusion coefficient in the case of P3 and P4 as the RH increased suggested swelling and not

Open Access Article. Published on 06 Juli 2021. Downloaded on 13.02.26 17:52:21.
This article is licensed under a Creative Commons Attribution 3.0 Unported Licence.

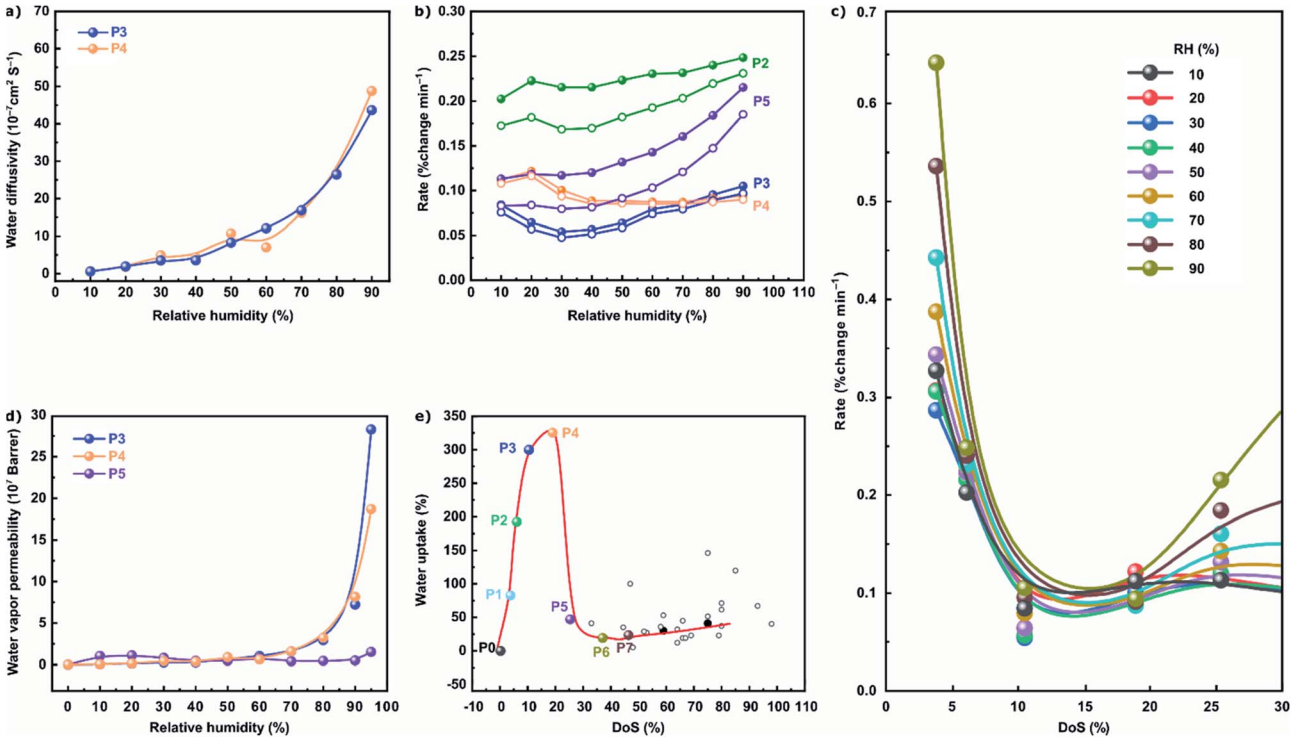

Fig. 6 (a) Water diffusivity as a function of RH for P3 and P4; (b) rate of adsorption relative to RH over 5 min (filled circles) and 10 min (empty circle); (c) adsorption rate *vs.* DoS at different RHs; (d) estimated water vapor permeability for P3, P4, and P5 at different RHs; and (e) water uptake performance of SPEEKs relative to the previously reported data (Table S7, ESI†), where filled and empty symbols indicate water vapor uptake and liquid water uptake, respectively.

cluster formation. The main driving force for the swelling/cluster formation was hydrogen bonding interactions. Fig. S3 (ESI)† shows a substantial increase in the hydrogen bonding interactions as the RH increased, which was consistent with the sorption data.

Water vapor sorption dynamics were assessed to elucidate the water uptake kinetics at 25 °C and varying RHs. The polymers were not dehydrated between each kinetic analysis to mimic the industrial application of the previously developed polymer adsorbents. SPEEKs exhibited a higher water uptake rate than nonsulfonated PEEKs measured at various time intervals (Fig. S4–S11, ESI†). With the exception of P4, at fixed time intervals of 5 and 10 min (Fig. 5b), the water uptake rate gradually increased as a function of the RH. In the case of P2, a high water uptake rate was realized at 90% RH within the first 5 min and a sorption uptake rate of 0.25% change min^{-1} was achieved. Although the water sorption isotherms showed high uptake for P3 and P4, the polymers suffered from a lower uptake rate than P2 and P5. The time interval of 10 min also revealed a similar trend of water uptake rate for all four SPEEKs (Fig. 6b, empty symbols). Importantly, our findings demonstrate the successful utilization of the developed adsorbents in short cycle times of only 5 min. The analysis of the water uptake rate as a function of DoS (Fig. 6c) revealed an interesting feature of the SPEEK adsorbents.

A decrease in the water uptake rate was observed with an increase in DoS. However, at a DoS of 10% and 19%, the rate became more stable, regardless of the RH. This is a significant feature of the adsorbents, indicating that SPEEKs can operate over the entire range of humidity without any significant loss in performance. This feature also indicates the utility of the developed polymer system in other applications, *e.g.*, atmospheric water harvesting. To predict the performance of the proposed system as a potential membrane material, we calculated the water vapor permeability of a 1 μm-thick membrane using diffusion coefficients. P3 and P4 exhibited a significant increase in the water vapor permeability with increasing RH (Fig. 6d).

When the RH was increased from 30% to 60% and from 60% to 90%, the water vapor permeability of P3 increased by three and seven times, respectively. However, at 95% RH, the water vapor permeability increased more than an order of magnitude. The same trend was also noted for P4. The results obtained herein agree with the literature on other polymers exhibiting high water permeance at high RHs.[35,36] P3 and P4 showed significantly higher water vapor permeability than P5 owing to their high water vapor sorption (Fig. 3a). The water vapor permeability achieved in this work is nearly two orders of magnitude higher than that of a previously reported SPEEK with a DoS of 60%.[37] This observation confirmed our hypothesis that the DoS of polymers must be carefully tuned and not necessarily maximized.

To predict the selectivity, we considered N_2 gas permeability to be 0.02 barrer.[38] However, in this work, the DoS was lower,

Open Access Article. Published on 06 Juli 2021. Downloaded on 13.02.26 17:52:21.
This article is licensed under a Creative Commons Attribution 3.0 Unported Licence.

which would result in lower N_2 gas permeability. The theoretical water vapor/N_2 selectivity obtained herein was remarkably high, *i.e.*, between 10^9 and 10^{11} (Fig. S12, ESI†).[8,39] A combination of very high water vapor permeability and selectivity was achieved. These results demonstrated the potential of SPEEK-based membranes with tunable properties for gas dehydration applications such as dehumidification.

Fig. 6e shows the water uptake as a function of DoS at 95% RH. In the graph, the data acquired herein are compared with those previously reported for other SPEEKs (Table S7, ESI†). In the case of P3 and P4, our polymer system showed a high water uptake at very low DoS (10% and 19%, respectively). The literature data on polymers with high DoS intersected the fitted curve, verifying our findings on the need to limit the DoS instead of maximizing it.

Conclusions

In summary, we proposed a new strategy for the design and preparation of various SPEEKs. Compared with other desiccants, the obtained polymers exhibited distinctive water vapor adsorption properties. The synthesized polymers were evaluated and classified based on the interactions within them and with water molecules. Markedly, based on their high performance, SPEEKs with very low DoS could be used as adsorbents for moisture control applications. However, when increasing the DoS from 19%, the sorption uptake began to decrease until reaching performance comparable to that of a polymer without any sulfonation. The MD simulations and NMR analysis confirmed this unique property based on the distance between two S atoms. The MD simulations and cluster formation calculated from the sorption isotherms revealed that once the DoS plateau was achieved, the interactions between the water vapor and polymer chains became weak as the DoS increased. An increase in sulfonation led to adverse effects, resulting in decreased water uptake. SPEEKs with a DoS in the range of 10–19% maintained high sorption integrity of more than 300% with a distinctive water vapor permeability. These remarkable features demonstrated that designing SPEEKs with tunable performance is beneficial. Based on these findings as well as the simple strategy used for synthesizing SPEEKs described herein, we believe that the developed adsorbents and membranes exhibiting outstanding performance can be utilized in energy-efficient air dehydration systems.

Conflicts of interest

There are no conflicts to declare.

Acknowledgements

The research reported in this publication was supported by funding from King Abdullah University of Science and Technology (KAUST), Kingdom of Saudi Arabia. The postdoctoral fellowship from the Advanced Membranes and Porous Materials Center at KAUST is gratefully acknowledged (MAA). The authors acknowledge the KAUST Cooling Initiative grant REP/1/3988-06-01.

References

1 V. Sagar and P. S. Kumar, *J. Food Sci. Technol.*, 2010, **47**, 15–26.
2 P. Scovazzo and A. J. Scovazzo, *Appl. Therm. Eng.*, 2013, **50**, 225–233.
3 M. Sultan, I. I. El-Sharkawy, T. Miyazaki, B. B. Saha and S. Koyama, *Renewable Sustainable Energy Rev.*, 2015, **46**, 16–29.
4 W. Goetzler, R. Zogg, J. Young and C. Johnson, *ASHRAE J.*, 2014, **56**, 12.
5 D. Jani, M. Mishra and P. Sahoo, *Renewable Sustainable Energy Rev.*, 2016, **60**, 1451–1469.
6 A. C. Rotzetter, C. M. Schumacher, S. B. Bubenhofer, R. N. Grass, L. C. Gerber, M. Zeltner and W. J. Stark, *Adv. Mater.*, 2012, **24**, 5352–5356.
7 A. J. Marszal, P. Heiselberg, J. S. Bourrelle, E. Musall, K. Voss, I. Sartori and A. Napolitano, *Energy Build.*, 2011, **43**, 971–979.
8 F. H. Akhtar, H. Vovushua, L. F. Villalobos, R. Shevate, M. Kumar, S. P. Nunes, U. Schwingenschlögl and K.-V. Peinemann, *J. Membr. Sci.*, 2019, **572**, 641–649.
9 Q. Chen, M. Burhan, M. W. Shahzad, D. Ybyraiymkul, F. H. Akhtar and K. C. Ng, *Energy Convers. Manage.*, 2020, **221**, 113169.
10 A. Jentys, G. Warecka, M. Derewinski and J. A. Lercher, *J. Phys. Chem.*, 1989, **93**, 4837–4843.
11 A. A. Pesaran and A. F. Mills, *Int. J. Heat Mass Transfer*, 1987, **30**, 1037–1049.
12 R. G. AbdulHalim, P. M. Bhatt, Y. Belmabkhout, A. Shkurenko, K. Adil, L. J. Barbour and M. Eddaoudi, *J. Am. Chem. Soc.*, 2017, **139**, 10715–10722.
13 A. J. Rieth, S. Yang, E. N. Wang and M. Dincă, *ACS Cent. Sci.*, 2017, **3**, 668–672.
14 A. Cadiau, Y. Belmabkhout, K. Adil, P. M. Bhatt, R. S. Pillai, A. Shkurenko, C. Martineau-Corcos, G. Maurin and M. Eddaoudi, *Science*, 2017, **356**, 731–735.
15 H. Furukawa, F. Gandara, Y.-B. Zhang, J. Jiang, W. L. Queen, M. R. Hudson and O. M. Yaghi, *J. Am. Chem. Soc.*, 2014, **136**, 4369–4381.
16 N. Hanikel, M. S. Prévot and O. M. Yaghi, *Nat. Nanotechnol.*, 2020, 1–8.
17 Y.-L. Wong, J. Tobin, Z. Xu and F. Vilela, *J. Mater. Chem. A*, 2016, **4**, 18677–18686.
18 Y. Byun, S. H. Je, S. N. Talapaneni and A. Coskun, *Chem.–Eur. J.*, 2019, **25**, 10262–10283.
19 Y. Byun and A. Coskun, *Angew. Chem., Int. Ed.*, 2018, **57**, 3173–3177.
20 D. R. Morris and X. Sun, *J. Appl. Polym. Sci.*, 1993, **50**, 1445–1452.
21 T. A. Zawodzinski Jr, C. Derouin, S. Radzinski, R. J. Sherman, V. T. Smith, T. E. Springer and S. Gottesfeld, *J. Electrochem. Soc.*, 1993, **140**, 1041.
22 K. Kreuer, *J. Membr. Sci.*, 2001, **185**, 29–39.

Open Access Article. Published on 06 Juli 2021. Downloaded on 13.02.26 17:52:21.
This article is licensed under a Creative Commons Attribution 3.0 Unported Licence.

23 L. Jia, X. Xu, H. Zhang and J. Xu, *J. Appl. Polym. Sci.*, 1996, **60**, 1231–1237.
24 R. S. Yee, K. Zhang and B. P. Ladewig, *Membranes*, 2013, **3**, 182–195.
25 A. G. Al Laf, *Polym. Degrad. Stab.*, 2014, **105**, 122–133.
26 D. Puhan, J. S. S. Wong and D. Puhan, *Tribol. Int.*, 2019, **135**, 189–199.
27 P. Xing, G. P. Robertson, M. D. Guiver, S. D. Mikhailenko, K. Wang and S. Kaliaguine, *J. Membr. Sci.*, 2004, **229**, 95–106.
28 K. Hadjiivanov, *Adv. Catal.*, 2014, **57**, 99–318.
29 M. A. Abdulhamid, G. Genduso, X. Ma and I. Pinnau, *Sep. Purif. Technol.*, 2021, **257**, 117910.
30 P. Zuo, Y. Li, A. Wang, R. Tan, Y. Liu, X. Liang, F. Sheng, G. Tang, L. Ge and L. Wu, *Angew. Chem., Int. Ed.*, 2020, **59**, 9564–9573.
31 M. A. Abdulhamid, S.-H. Park, H. Vovusha, F. H. Akhtar, K. C. Ng, U. Schwingenschlögl and G. Szekely, *J. Mater. Chem. A*, 2020, **8**, 24445–24454.
32 G. Ye, N. Janzen and G. Goward, *Macromolecules*, 2006, **39**, 3283–3290.
33 E. M. Davis and Y. A. Elabd, *J. Phys. Chem. B*, 2013, **117**, 10629–10640.
34 F. H. Akhtar, M. Kumar, H. Vovusha, R. Shevate, L. F. Villalobos, U. Schwingenschlögl and K.-V. Peinemann, *Macromolecules*, 2019, **52**, 6213–6226.
35 S. Koester, F. Roghmans and M. Wessling, *J. Membr. Sci.*, 2015, **485**, 69–78.
36 H. Azher, C. A. Scholes, G. W. Stevens and S. E. Kentish, *J. Membr. Sci.*, 2014, **459**, 104–113.
37 H. Sijbesma, K. Nymeijer, R. van Marwijk, R. Heijboer, J. Potreck and M. Wessling, *J. Membr. Sci.*, 2008, **313**, 263–276.
38 H. Azher, C. Scholes, S. Kanehashi, G. Stevens and S. Kentish, *J. Membr. Sci.*, 2016, **519**, 55–63.
39 T. Puspasari, F. H. Akhtar, W. Ogieglo, O. Alharbi and K.-V. Peinemann, *J. Mater. Chem. A*, 2018, **6**, 9271–9279.

 This journal is © The Royal Society of Chemistry 2021